Aalborg Universitet

The paddlewheel complex of 1,8-naphthyridine and palladium(II)

Nielsen, Mathias T.; Mihrin, Dmytro; Jørgensen, Mike S.B.; Yan, Xiaomei; Berg, Rolf W.;
Xiao, Xinxin; Larsen, René Wugt; Nielsen, Martin

Link to publication from Aalborg University

The paddlewheel complex of 1,8-naphthyridine and palladium(II)

Mathias T. Nielsen [a],[2], Dmytro Mihrin [a],[3], Mike S.B. Jørgensen [a],[4], Xiaomei Yan [a],[b],[5], Rolf W. Berg [a],[6], Xinxin Xiao [a],[c],[7], René Wugt Larsen [a],[8], Martin Nielsen [a],[*],[1]

[a] *Department of Chemistry, Technical University of Denmark, DK-2800 Kgs Lyngby, Denmark*
[b] *Lanzhou Institute of Chemical Physics, Chinese Academy of Sciences, Lanzhou 730000, Gansu, China*
[c] *Department of Chemistry and Bioscience, Aalborg University, DK-9220 Aalborg, Denmark*

ABSTRACT

This work presents the synthesis of the tetracationic paddlewheel complex of 1,8-naphthyridine and palladium (II), $[Pd_2(\mu\text{-napy})_4]X_4$, ($X = BF_4^-$ or PF_6^-). Single-crystal X-ray diffraction confirms a D_{4h} symmetric paddlewheel structure encompassing the two Pd units in the metal core coordinated by four ditopic 1,8-naphthyridine ligands, featuring a relatively short Pd–Pd distance. Spectroscopic analyses combined with density-functional theory (DFT) provide insights into the nature of the Pd–Pd and Pd–Napy interactions as well as observed optical absorption frequencies.

1. Introduction

Paddlewheel complexes are bimetallic coordination compounds, often found bearing rigid anionic ligands [1], such as halides [2,3], amidinates [4,5], pyrophosphite [6,7], carboxylates [8], and guanadinate derivatives [9,10] of which the anion of triazabicyclodecene (hpp), has been shown to aptly stabilize (strongly) oxidizing metal centers [11]. Paddlewheel complexes have been shown to demonstrate a distinctive reactivity relative to their monometallic analogues, exemplified by the early work of Gray on the oxidative additions of I_2 and MeI to the dicationic Rh(I)-dimer $[Rh_2(\mu\text{-}1,3\text{-diisocyanopropane})_4][BPh_4]_2$ [12], as well as Fackler's extensive work on digold(I) complexes [13]. More recently, paddlewheel complexes of late-transition metals are well-described (pre)catalysts towards the functionalization of C–H bonds [14–18], where a combination of metal-proximity and the nature of the ligand affects the oxidation potential rendering such transformations possible. Relevant to these transformation is Budnikova's study on trends in the redox chemistry of cyclometalated (di)palladium

(II) complexes, which reveals a correlation between Pd–Pd distance and oxidation potential, showing that the shorter Pd–Pd distance results in complexes with a lower oxidation potential [19]. Many of these complexes bear formally anionic ligands, and as such, it is of interest to investigate the (electro)chemical properties of paddlewheel complexes bearing formally neutral ligands unsupported by a metal–metal bond. Specifically, whether such complexes support the formation of metal–metal bond(s) through oxidation or reduction. In this context, 1,8-naphthyridine (abbreviated napy) is of interest as the close disposition of the two parallel *N*-centered lone pairs furnish the formation of several homoleptic [20–25] and heteroleptic [26–33] dinuclear complexes bearing the napy ligand. Similarly, there are also examples of napy coordinating as a bidentate [34] and as a monodentate ligand [21,35]. Additionally, through the introduction of imine functionalities to the parent bicyclic structure, Uyeda and co-workers have recently demonstrated several transformations [36–38] mediated by a dinickel complex bearing a redox non-innocent ligand [39]. Broere and co-workers have similarly effected novel properties of metal complexes bearing a

---

* Corresponding author.
E-mail address: marnie@kemi.dtu.dk (M. Nielsen).
[1] orcid.org/0000-0002-3170-1198.
[2] orcid.org/0000-0002-1928-5128.
[3] orcid.org/0000-0002-2594-7028.
[4] orcid.org/0000-0002-6968-1225.
[5] orcid.org/0000-0003-1882-4713.
[6] orcid.org/0000-0002-3195-1867.
[7] orcid.org/0000-0002-0240-0038.
[8] orcid.org/0000-0003-2983-6795.

modified napy-ligand: the introduction of phosphine moieties results in the ability of the ligand-framework to partially dearomatize leading to interesting properties, as for instance observed in a proton-responsive dicopper complex [40,41], as well as a low-valent diiron complex mediating proton-coupled electron-transfer reactions [42].

In this work, we explore the use of the unmodified napy ligand to furnish the formation of the cationic dipalladium(II)-tetranapy paddlewheel complexes $[Pd_2(\mu\text{-napy})_4][BF_4]_4$ and $[Pd_2(\mu\text{-napy})_4][PF_6]_4$. The spectroscopic and electrochemical properties of the Pd_2^{4+} complex are addressed by various analytical means.

2. Results and discussion

2.1. Synthesis and solid-state structure

As outlined in Scheme 1, the addition of napy to a solution of tetrakis (acetonitrile) palladium(II) tetrafluoroborate, $[Pd(MeCN)_4][BF_4]_2$, or hexafluorophosphate $[Pd(MeCN)_4][PF_6]_2$, yields the corresponding tetracationic paddlewheel-dipalladium complex, tetra-μ-napy-dipalladium(II) tetrafluoroborate, $[Pd_2(\mu\text{-napy})_4][BF_4]_4$ (**1**) and tetra-μ-napy-dipalladium(II) hexafluorophosphate (**2**). Both complexes **1** and **2** show a diamagnetic behavior from well-resolved NMR spectra (^{1}H, ^{13}C, ^{19}F, and ^{31}P), which further reflects a high symmetry from the presence of only three resonances in the ^{1}H NMR spectrum, *cf.* Figs. S1 and S6. During oxidation and reduction experiments we were able to isolate Pd-salts that demonstrated six resonances accounting for four individual and two overlapping peaks, one for each of the C2 through C7 position of the napy-backbone, following extrusion of a Pd ion from the paddlewheel complex. Moreover, in our pursuit of preparing the diplatinum(II) congener under the same conditions, we instead isolated the dicationic salt tetra-(κ-*N*-napy) platinum(II) hexafluorophosphate, $[Pt(napy)_4]$ $[PF_6]_2$. This complex features a ^{1}H NMR spectrum which demonstrates this splitting pattern of napy, as shown in Fig. S1 0, and these findings are in agreement with those reported by Biffis [25]. The salts of complexes **1** and **2** are stable upon exposure to air, moisture, and light. The molecular structure of the paddlewheel core of complex **1** is depicted in Fig. 1, and shows that each palladium(II) center of complex **1** is coordinated in a square planar fashion by four symmetry-equivalent napy ligands in a paddlewheel geometry.

From Table 1, the average Pd–N bond length is 2.04 Å and the Pd–Pd separation is significantly shorter than the sum of the van der Waals radii of 3.42 Å [43]. While these distances compare well to the platinum congener, $[Pt_2(\mu\text{-napy})_4][OTf]_4$ [25], they are on average expectedly shorter. $[Pt_2(\mu\text{-napy})_4][OTf]_4$ features average bond distances of Pt-N (napy) 2.05 Å and a Pt–Pt' separation of 2.58 Å, respectively. The napy ligands in **1** bridge the two metal centers planarly, as in the molybdenum [30], rhodium [24], and platinum [25] analogues. Finally, a comparison of the distances of **1** to that of the neutral dipalladium(II) triazabicyclodecene (hpp) complex reported by Cotton [10] reveals more comparable bond distances, as this complex features an average Pd–N (hpp) bond length of 2.04 Å and Pd–Pd' separation of 2.55 Å. Selected bonding parameters are presented in Table 1, and a full list of bond lengths, angles, and torsion angles are provided in Table S1 through Table S3.

To better understand the electronic structure of the core of the
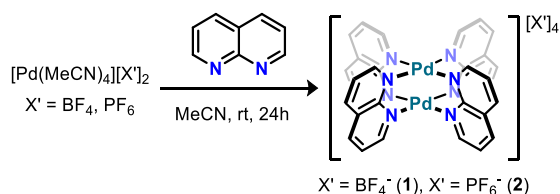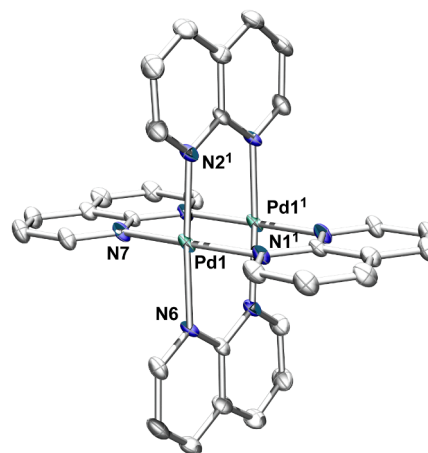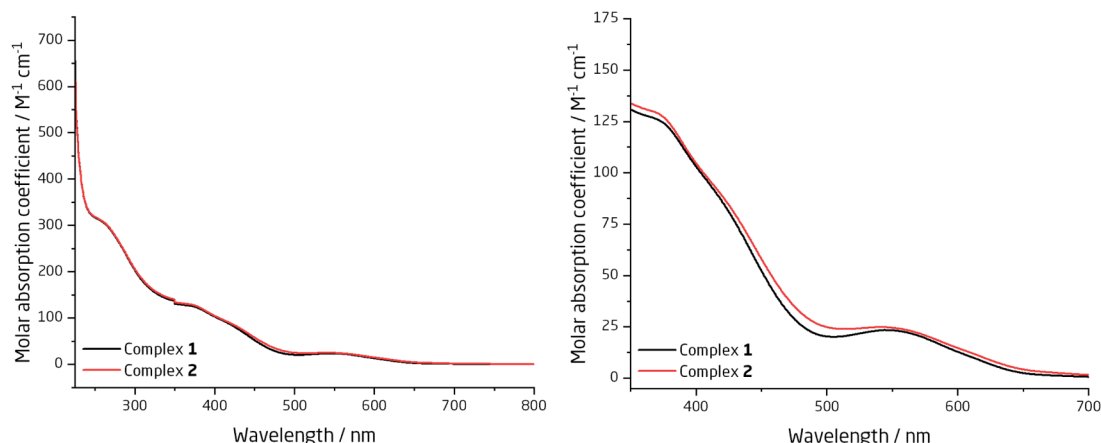

Fig. 1. Solid-state structure of complex 1. Thermal ellipsoids are plotted at 50 % probability level. BF$_4$-counterions, co-crystallized MeCN, and H-atoms are omitted for clarity. Color coding: C grey, N blue, Pd sea green.

Table 1
Selected bonding parameters of **1**.

Bond lengths (Å) and angles (deg) in the solid-state structure	
Pd1-Pd1[1]	2.5644(6)
Pd1-N6	2.043(3)
Pd1-N7	2.054(3)
Pd1-N2[1]	2.041(3)
Pd1-N1[1]	2.035(3)
N6-Pd1-N7	90.51(13)
N7-Pd1-N2[1]	90.40(13)
N2[1]-Pd1-N1[1]	89.34(13)
N1[1]-Pd1-N6	89.18(13)
N1[1]-Pd1-N7	174.40(13)
N2[1]-Pd1-N6	174.05(13)

paddlewheel complex, specifically the nature of the Pd–Pd interaction, given the short metal–metal distance and the high symmetry of the complex, optical absorption spectroscopy in DMF was carried out for complexes **1** and **2**, which is shown in Fig. 2. Both spectra feature an absorption in the visible region around 550 nm (ε(550 nm (λ_{max})) = ~25 M^{-1} cm^{-1}) and further absorptions are present in the UV-region, likely relating to intraligand transitions. In this context, various dinuclear napy-complexes feature strong metal-to-ligand charge transfer (MLCT) in the region from 450 to 330 nm [20,22]. In the visible region, the analogous dimolybdenum(II) napy complex, $[Mo_2(\mu\text{-napy})_4(MeCN)_2]^{4+}$, features a low-energy transition (λ = 699 nm, ε = 717 M^{-1} cm^{-1}), which the authors assign to a $\delta \rightarrow \delta^*$ transition [30]. Differently, in the tetraformamidinato dipalladium(II) complex, Pd$_2$(μ-DAni)$_4$ (DAni = *N*,*N'*-di-*p*-anisylformamidinate), a low-energy transition ($\lambda \sim 500$ nm) is observed, which upon oxidation to the corresponding Pd$_2^{5+}$-core disappears [44,45]. To further explore the observed transition, we sought to apply DFT to better understand the electronic properties of complex **1** [46,47]. Fig. S11 shows the frontier-molecular orbitals of the ground-state: the HOMO comprises an antibonding interaction (σ^*) between two Pd atomic $d(z^2)$ orbitals, whereas the LUMO comprises an antibonding interaction between the two atomic d (x^2-y^2) orbitals and the ligands (σ^*(M-L), $d(x^2$-y^2)-L(σ^*)). This observation is consistent with d^8-d^8 interactions reported in other Pd^{II} dimers [48], and these orbitals formed the basis for our time-dependent DFT (TD-DFT) analysis, where we have been able to discern a trend that accounts for the orbitals relevant to the observed excitation in Fig. 2. In vacuum, the quantum chemical calculations predict two transitions: a low-energy, low-intensity transition, at 484 nm, followed by a high-energy transition at 338 nm. We suggest that the former transition

Scheme 1. Synthesis of the paddlewheel complexes 1 and 2 starting from Pd (II) acetonitrile adducts.

Fig. 2. Optical absorption spectra of paddlewheel complexes **1** and **2** as 10 mM solutions in DMF. The left-hand graph shows the full spectrum ranging from 225 to 800 nm. The right-hand graph shows a selected region between 350 and 700 nm, focusing on specific absorptions relevant to visible light. Change in light-source occurs at 350 nm.

relates to a metal–metal to ligand charge transfer (MMLCT) transition [48], as it comprises a transition from the HOMO to LUMO+2 and LUMO+3 (degenerate), whereas the higher-energy transition is more consistent with an intraligand transitions from HOMO−1 to LUMO+3. Additionally, to account for a polar solvation shell relevant to the experimentally observed excitation, which potentially could stabilize an excited charge-distribution centered on the ligand, two implicit solvation models were investigated, using DMF as solvent: conductor-like polarizable continuum model (CPCM), and cavity-dispersion-solvent structure (CDS) term, respectively. These calculations suggest the UV transition redshifts to 590 nm, which, despite a somewhat crude model, provides some insight into how solvent polarity affects the spectrum. Additionally, Fig. S13 compares the UV–Vis spectrum of complex **1** in MeCN and DMF, showing that the same transition slightly red-shifts with increasingly polar solvent. Based on these findings, we suggest that the absorption spectrum of complex **1** displays a MMLCT transition rather than a pure *d-d* transition in addition to intraligand transitions.

2.2. FIR, Raman, and DFT-calculated spectra

The complete vibrational spectrum of the free napy ligand has previously been reported in a combined Raman/infrared investigation of napy embedded in a Nujol mull [49] and later in a surface-enhanced Raman spectroscopic (SERS) investigation of napy adsorbed on silver colloids [50]. The attenuated-total-reflectance (ATR) spectra of **1** collected in the mid-infrared fingerprint (600–1700 cm^{-1}) and the far-infrared (150–600 cm^{-1}) spectral regions are shown in Fig. 3. The complementary plot shown the mid- and far-infrared spectral regions of complex **2** is shown in Fig. S14. Similarly, the complementary Raman resonance of complex **2** is shown in Fig. S15. The mid-infrared region shown in Fig. 3 features mostly vibrational fundamental transitions associated with slightly perturbed intramolecular normal modes of the napy ligands, whereas the far-infrared part of the spectra additionally exhibits several fundamental transitions associated with large-amplitude vibrational motion involving the metal–ligand bonds. Our infrared and Raman spectroscopic observations for **1** agree rather well with the literature, although the mid-infrared part of the spectrum in the 900–1175 cm^{-1} range is blurred due to the very strong and broad absorption feature resulting from the B-F stretching modes of the BF$_4$ counter-ions. A complete list of observed infrared and Raman band positions of distinct bands is provided in the supplementary material, *c.f.* Tables S4. The far infrared spectrum shown in Fig. 4 reveals several absorption bands, which have previously been assigned to different modes involving the torsional and bending motion of the aromatic rings of the napy monomer [49,50].
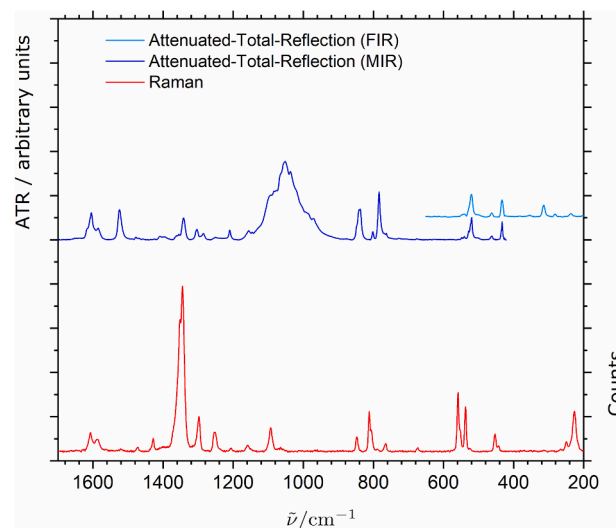
Fig. 3. The attenuated-total-reflectance (ATR) infrared (blue traces) and Raman spectra (red trace) of **1** in the mid-infrared fingerprint and the far-infrared spectral regions.

Three bands observed at 169, 433, and 463 cm^{-1}, respectively, relates directly to the torsional motions of the ring, and gain intensity in napy due to the asymmetry introduced by the *N*-heteroatoms. Additionally, the two bands observed at 521 and 543 cm^{-1}, respectively, have both previously been assigned to bending motions of the aromatic rings [49,50]. More interestingly, the observed three distinctive vibrational transitions, not previously observed in monomeric napy, at 236, 281 and 314 cm^{-1}, respectively, are indicative of the complexation between the napy ligands and Pd(II). Some ambiguity exists on the particular far-infrared assignments of the N···Pd···N bending and Pd···N stretching modes for palladium(II) complexes, as different studies have assigned vibrational transitions associated with large-amplitude Pd···N stretching modes in the 400–550 cm^{-1} range [51] and other investigations have assigned these stretching transitions in the 200–300 cm^{-1} range [52]. However, a normal mode analysis of the present harmonic vibrational predictions at the TPSS-D4/def2-TZVP [Pd def2-QZVP] level of theory provides further insight into the observed transitions. The theoretical simulation of the far-infrared spectrum based on this level of theory is shown in Fig. 4 together with the experimental spectrum. Two observed transitions at 236 and 314 cm^{-1}, respectively,
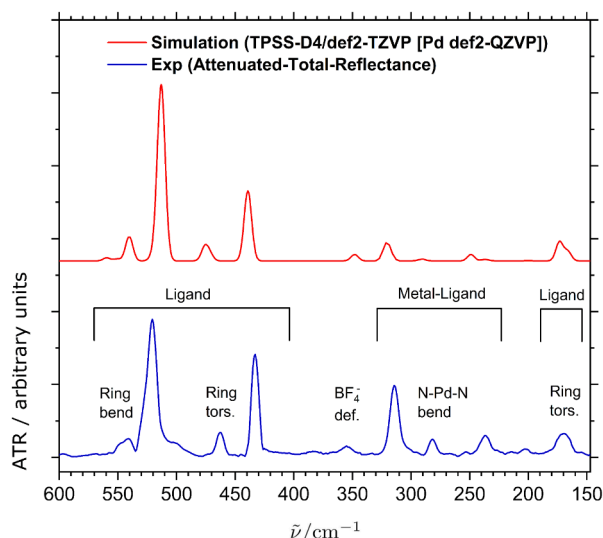
Fig. 4. Experimentally observed far-infrared attenuated-total-reflectance spectrum of **1** (blue trace) together with a simulation of the spectrum at the TPSS-D4/def2-TZVP [Pd def2-QZVP] level of theory (red trace).

are associated with two different concerted out-of-plane N⋯Pd⋯N bending modes involving all four napy subunits. A third transition at 281 cm^{-1} is associated with a concerted in-plane N⋯Pd⋯N bending mode. A normal mode animation of the highest-energy out-of-plane N⋯Pd⋯N bending mode is illustrated in Fig. 5.

Based on the predicted Raman activities at the same level of theory, we tentatively assign the vibrational transition observed at 673 cm^{-1} in the Raman spectrum to a concerted large-amplitude N⋯Pd⋯N stretching motion involving all the metal–ligand bonds. The normal mode animation of the predicted vibrational motion (with three-fold amplified vibrational displacements) is shown in Fig. 6, which demonstrates that this concerted N⋯Pd⋯N stretching motion does not involve any change of the overall dipole moment and is therefore only (slightly) Raman-active. The agreement between the DFT simulation and experiment is surprisingly good although the undertaken harmonic vibrational predictions are more challenging for the N⋯Pd⋯N bending modes due to the more anharmonic character for this class of large-amplitude vibrational motion.

2.3. Electrochemical studies

We investigated the electrochemical properties of [Pd$_2$(μ-napy)$_4$]$^{4+}$ to determine whether any distinct oxidation events, consistent with the formation of (transient) Pd^{II}Pd^{III} or a Pd$_2^{6+}$ species, could be observed. Cyclic voltammograms (CVs) were obtained for both napy and [Pd$_2$(μ-napy)$_4$][PF$_6$]$_4$ in DMF, as shown in top of Fig. 7, as well as for [Pd$_2$(μ-napy)$_4$][BF$_4$]$_4$ in MeCN, although the latter spectrum is difficult to fully interpret, see Fig. S16. The CVs in the top of Fig. 7 suggest to us that the

observed redox events are related to the paddlewheel complex, as no significant redox events were observed for napy alone (blue trace).

To better understand the redox processes in the CV at the bottom of Fig. 7, where the complex was examined at a higher concentration and varying scan rates, we attempted to isolate well-defined products resulting from oxidation and reduction of the parent dipalladium(II) complexes **1**/**2**, respectively. However, no such species were obtained in our hands. Instead, we recovered unreacted starting material, indicating minimal consumption of the starting material, along with monopalladium complexes ligated by napy, and byproducts from napy-oxidation. We therefore suggest that the oxidation event observable in voltammogram of Fig. 7 is not metal centered. Similarly, the nature of the three distinct reduction events remains unclear, and more likely relate to the initial oxidation event.

3. Conclusion

In closing, we demonstrate that napy tethers two Pd(II) ions closely together resulting in new, distinctive electrochemical properties.

Spectroscopic and computational analysis suggests that despite a close Pd–Pd distance the proximity does not constitute a formal bond, following a full population of bonding and antibonding metal–metal molecular orbitals of mainly M-$d(z^2)$ character as disclosed by optical absorption spectroscopy combined with TD-DFT. Combining far-infrared spectroscopy with DFT enable us to understand and ascertain the N-Pd–N bending transitions, resolving some existing ambiguity. Finally, we find that the napy ligand poorly supports strongly oxidizing metal-centres, as neither complex **1** nor **2** work as synthons for the isolation of Pd^{II}Pd^{III} and Pd$_2^{6+}$ complexes. Neither have we been able to isolate dipalladium complexes of lower valency.

4. Experimental

4.1. General considerations and instrumentation

All syntheses were performed in air unless otherwise specified. Handling of air-sensitive reagents was conducted under inert gas conditions using standard Schlenk or glovebox techniques in an Argon-filled Inert glovebox. Most chemicals were commercially achieved and used without further purification as received from Strem Chemicals (PdCl$_2$, PdBr$_2$, PdI$_2$) and FluoroChem (napy, [Pd(MeCN)$_4$][BF$_4$]$_2$, AgPF$_6$, and AgBF$_4$). We found that the long-term storage of AgPF$_6$ under inert conditions is important to prevent its hydrolysis. Elemental analyses were acquired by the Micro Analytical Laboratory at the Department of Chemistry, University of Copenhagen on a Thermo Fisher FlashEA 1112 analyzer. All handling was conducted under ambient conditions.

4.2. Nuclear Magnetic Resonance Spectroscopy (NMR)

^{1}H, ^{13}C, ^{19}F, and ^{31}P NMR spectra were recorded on Bruker Ascend spectrometer with a Prodigy cryoprobe operating at 400 MHz for ^{1}H NMR, 101 MHz for ^{13}C, for 377 MHz ^{19}F NMR, and 162 MHz for ^{31}P
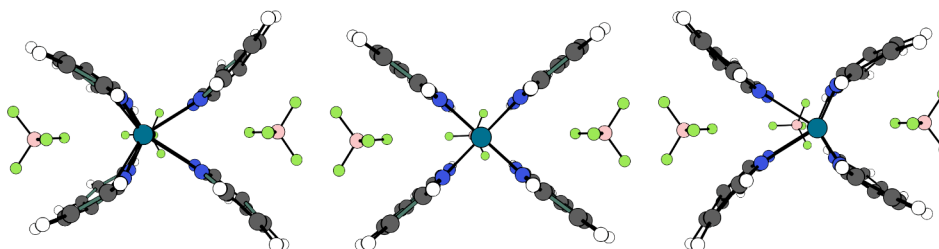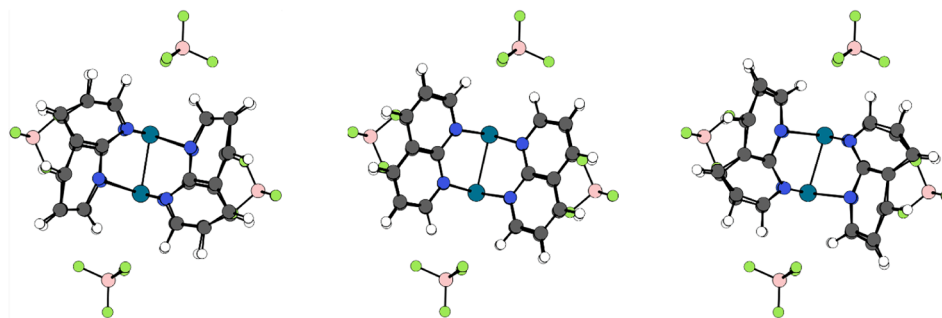

Fig. 5. The animation of the large-amplitude concerted out-of-plane N⋯Pd⋯N bending mode of **1**, with the equilibrium configuration of **1** shown (center) together with the configurations at the two outer vibrational turning points of the normal mode (left and right). The front BF$_4$ counter-ion is omitted for clarity.

Fig. 6. The animation of a large-amplitude concerted N⋯Pd⋯N stretching mode of **1**, with the equilibrium configuration of **1** shown (center) together with the configurations at the two outer vibrational turning points of the normal mode (left and right).
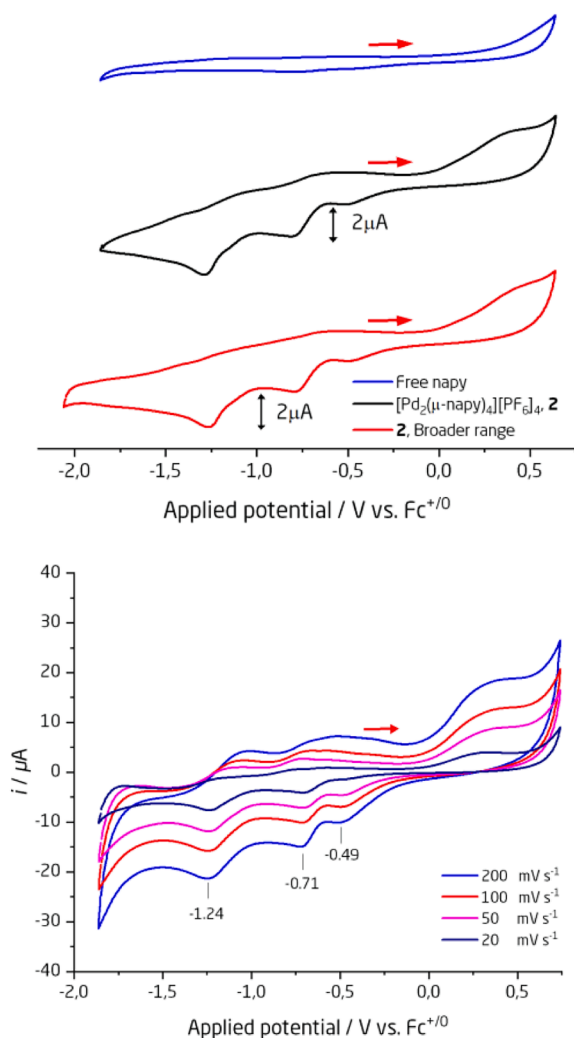
Fig. 7. The top voltammogram shows napy and $[Pd_2(\mu\text{-napy})_4][PF_6]_4$ (complex **2**) at 0.25 mM concentration in DMF, and at 20 mV s^{-1}, suggesting that the redox properties are a consequence of the complexation between Pd and napy. The lower figure shows a voltammogram of complex **2** at various scan rates.

NMR. ^{1}H and ^{13}C chemical shifts are reported relative to SiMe$_4$, using the residual solvent peak as internal reference [53]. The specific deuterated solvent is stated for each compound. NMR spectra were analysed using MestReNova software.

4.3. Infrared spectroscopy (AT-IR and FTIR) and Raman spectroscopy

The collected attenuated-total-reflectance (ATR) Fourier Transform infrared (FTIR) spectra have been obtained by a VERTEX 80 vacuum FTIR spectrometer from Bruker Optics GmbH. The mid-infrared spectral region (450–5000 cm^{-1}) was collected with a Ge on KBr beam splitter, a liquid nitrogen cooled HgCDTe detector and an air-cooled thermal global radiation source employing a single-reflection germanium ATR accessory (IRIS) from PIKE Technologies Inc. The far-infrared (100–500 cm^{-1}) recordings were done with a multilayer Mylar beamsplitter, a room temperature DTGS detector and a water-cooled thermal Globar radiation source employing a single-reflection diamond ATR accessory. The collected spectra of 2 cm^{-1} spectral resolution have been corrected for small traces of residual water vapor absorption from the interferometer and the resulting absorption spectra have been corrected for minor baseline drifts. Subsequently, extended ATR corrections have been applied to account for the wavelength-dependent penetration depth of the infrared probe beam into the solid sample.

The Raman spectra were collected employing the visible lines at 514.5 nm (green) and 488.0 nm (blue) emitted from a LEXEL 95-SHG-QS Argon ion laser (Cambridge Laser Laboratories Inc., USA) as the excitation sources. The continuous laser power was adjusted to ~4 mW, of which about half or less reached the uncovered surface of the sample to avoid sample oxidation. The excitation laser was passing through an InVia Reflex Raman instrument (Renishaw plc, England) via mirrors to an attached Leica DM2700M microscope (Leica Microsysteme Vertrieb GmbH, Germany) equipped with a traditional X5 objective. The scattered light from the sample was collected and sent back through a high-pass filter system dispersed in a single stage spectrograph and detected with a Peltier-cooled high-sensitive CCD device. The entrance slit width was set to 55 μm and the acquisition condition was set to up to 100 s with automatic removal of cosmic spikes. Independent Raman spectra were collected and co-added. The resulting Raman spectrum was not manipulated further and not corrected for monochromator and detector efficiencies. The calibration of the absolute wavenumber scale was done with a diamond slab having its strongest band at ~1332.4 cm^{-1} and [54] the scale was checked with the ASTM bands of cyclohexane and polystyrene [55,56] to within 1–2 cm^{-1} accuracy.

4.4. Electrochemical measurements

Electrochemical measurements were recorded on an Autolab PGSTAT12 instrument (Eco Chemie, Switzerland) at room temperature (*ca.* 20 °C) with the glassy carbon electrode (GCE), a Pt wire, and a solid Ag/AgCl electrode as the working, counter, and reference electrode, respectively. Cyclic voltammetry (CV) was conducted in DMF and MeCN containing 0.1 M tetrabutylammonium hexafluorophosphate (TBAPF$_6$) with compound **1** or **2** in a potential range from −1.5 to 1.1 V versus Ag/AgCl at different scan rates of 20, 50, 100, 200, 400 and 500 mV s^{-1}. The potential was then calibrated to against the formal potential of Fc$^{+/}$

4.5. Single-crystal X-ray structure determination

A suitable crystal was harvested with a MiTeGen cryo loop and mounted on a goniometer attached to a SuperNova Dual Source CCD-diffractometer. Data were collected at the given temperature K using Cu Kα (**1**) radiation under a stream of N$_2$. Data integration ranging from 0.84 Å to 0.72 Å resolution was carried out using CrysAlis Pro software with reflection spot size optimization. Using Olex2 [57 1], the structure was solved with the olex2.solve [58] structure solution program using Charge Flipping and refined with the SHELXL [59] refinement package using Least Squares minimisation. The program PLATON was used to confirm an absence of missing symmetry elements. Non-hydrogen atoms were refined with anisotropic displacement parameters, and hydrogen atoms were added in idealized positions and refined using a riding model.

4.6. Computational methods

The quantum chemical calculations were performed using the ORCA (5.0) [60] software package. The optimized equilibrium geometry and the harmonic vibrational frequencies and Raman activities of the complex **1** molecular unit were calculated using the dispersion-corrected TPSS-D4 [61] functional together with the def2-TZVP [62–64] basis set (QZVPP basis set used for the Pd atoms). TD-DFT [65] calculations of the electronic excited states transition energies were performed using the TPSSh-D4 method with the def2-TZVPD (QZVPPD-Pd) [66] basis set on the corresponding potential energy minimum geometry of complex **1**$^{4+}$ ionic form of the compound. The solution has been obtained for the first 10 roots. The RIJ-COSX approximation was used for all calculations [67].

4.7. Synthetic methods

Complex **1** is readily prepared using commercially available [Pd (MeCN)$_4$][BF$_4$]$_2$, whereas the hexafluorophosphate precursor to obtain complex **2** has to be prepared from an initial halide abstraction performed in MeCN using a slight excess AgPF$_6$. This halide abstraction reaction similarly affords [Pd(MeCN)$_4$][BF$_4$]$_2$ when AgBF$_4$ is used as the abstractor, and any of the halides PdX$_2$ (X = Cl, Br, or I) work as a source of Pd(II).

Preparation of tetrakis(acetonitrile) palladium(II) tetrafluoroborate or hexafluorophosphate precursors. We found that this step can be performed in air when the filtrates are directly applied in complexation. 2.0 equivalent of PdX$_2$ (X = Cl, Br, or I) and 4.02 equivalents of dry AgX′ (X′ = BF$_4$ or PF$_6$) were weighed out into a round-bottom flask. The flask was added a stir bar, MeCN (30 mM with respect to Pd), fitted a reflux condenser, and the setup was covered in aluminum foil before it was placed in a pre-heated oil bath. The suspension was stirred at a gentle reflux for roughly three hours (six hours for PdI$_2$) turning bright yellow. The flask was cooled to room temperature, the suspension was filtered through a pad of celite, and the yellow filtrate transferred to another round-bottom flask charged with a stir bar.

Preparation of complexes **1** and **2**. This step may be performed in air. 4.05 equivalents of napy was added to the round-bottom flask containing the filtrate of 2.0 equivalent of [Pd(MeCN)$_4$][X′]$_2$ and the mixture stirred overnight at room temperature. The overnight stirring occasionally resulted in the formation of a white/yellow suspension within the first couple of hours, which overnight had disappeared. The following day, the slightly red/brown solution was collected via filtration and the white precipitate discarded. The filtrate was concentrated *in vacuo* to about 1–2 mL of solvent and Et$_2$O was added until the precipitation of a white/pink powder stopped. This solid was transferred onto

a glass frit, medium or fine coarseness and washed with 3 × 5 mL each of benzene and acetone. The powder was finally washed with small fractions (~1 mL at a time) of cold MeCN (0 °C) until the filtrate no longer was colored by any bright yellow colors. The powder was then washed with 5 mL of Et$_2$O and 5 mL of pentane, before the powder was left to dry in the air on the glass frit. Once dry, the powder redissolved in minimum amounts of MeCN and the slightly colored solution was collected and solvent was removed *in vacuo*, yielding the target dipalladium(II) complex as a slightly pinkish powder in good to excellent yield (50–68 %). 250 mg [Pd(MeCN)$_4$][BF$_4$]$_2$ gave 206.8 mg (68 %) of the resulting BF$_4$-complex. Using 250 mg PdCl$_2$ gave 601.8 mg (65 %) of the resulting PF$_6$-complex. Comparable yields of complexes **1** and **2** were obtained by using PdBr$_2$ and PdI$_2$.

Complex 1, the BF$_4$-salt. ^{1}H NMR (400 MHz, CD$_3$CN) δ 10.24 (broad singlet, 1H), 8.63 (d, J = 7.0 Hz, 1H), 8.03 (t, J = 7.0 Hz, 1H). ^{13}C NMR (101 MHz, CD$_3$CN) δ 161.73, 145.93, 130.04, 127.57. ^{19}F NMR (377 MHz, CD$_3$CN) δ −151.30, −151.35. ^{1}H NMR (400 MHz, DMSO-d_6) δ 10.35 (dd, J = 5.4, 1.7 Hz, 1H), 8.80 (dd, J = 8.2, 1.7 Hz, 1H), 8.15 (dd, J = 8.2, 5.4 Hz, 1H). ^{19}F NMR (377 MHz, DMSO-d_6) δ −148.26 (s, F-^{10}B), −148.31 (s, F-^{11}B). **Elemental analysis** calcd (%) for C$_{32}$H$_{24}$F$_{16}$N$_8$B$_4$Pd$_2$ · (2 MeCN, H$_2$O): C 36.62, H. 2.73, N. 11.86; found: C 36.56, H 2.67, N 11.75. **UV–Vis:** λ_{max} 544 nm, 37 (ε/M^{-1} cm^{-1}). Colorless single-crystals suitable for single-crystal X-ray diffraction were obtained by two means: 1) overnight by Et$_2$O vapor diffusion into a concentrated MeCN solution of complex **1** at −18 °C and 2) slow solvent evaporation of a concentrated sample in MeCN.

Complex 2, the PF$_6$-salt. ^{1}H NMR (400 MHz, DMSO-d_6) δ 10.36 (dd, J = 5.4, 1.7 Hz, 1H), 8.81 (dd, J = 8.2, 1.7 Hz, 1H), 8.15 (dd, J = 8.2, 5.4 Hz, 1H). ^{13}C NMR (101 MHz, DMSO-d_6) δ 160.0, 155.6, 144.0, 128.5, 125.9. ^{19}F NMR (377 MHz, DMSO-d_6) δ −70.17 (d, J = 712.1 Hz). ^{31}P NMR (162 MHz, DMSO-d_6) δ −144.18 (hept, J = 712.1 Hz). **Elemental analysis** calcd (%) for C$_{32}$H$_{24}$F$_{24}$N$_8$P$_4$Pd$_2$:C 29.27, H 1.84, N 8.53; found: C 29.24, H 1.85, N 8.53.

CRediT authorship contribution statement

Mathias T. Nielsen: Writing – review & editing, Writing – original draft, Visualization, Investigation, Formal analysis, Data curation, Conceptualization. **Dmytro Mihrin:** Formal analysis, Data curation. **Mike S.B. Jørgensen:** Formal analysis, Data curation. **Xiaomei Yan:** Formal analysis, Data curation. **Rolf W. Berg:** Formal analysis, Data curation. **Xinxin Xiao:** Formal analysis, Data curation. **René Wugt Larsen:** Formal analysis, Data curation. **Martin Nielsen:** Writing – review & editing, Supervision, Resources, Project administration, Funding acquisition, Conceptualization.

Declaration of competing interest

The authors declare the following financial interests/personal relationships which may be considered as potential competing interests: Martin Nielsen reports financial support was provided by Technical University of Denmark. Xinxin Xiao reports financial support was provided by Technical University of Denmark. If there are other authors, they declare that they have no known competing financial interests or personal relationships that could have appeared to influence the work reported in this paper.

Appendix A. Supplementary data

The electronic supporting information (ESI) contains ^{1}H, ^{13}C, ^{19}F,

and ^{31}P NMR spectra; Tabulated IR values and Raman resonances; Additional computational results; and additional electrochemical data. A .ZIP-file containing output files for 1) vibrational and 2) UV spectra and corresponding orbitals, as well as cartesian coordinates (XYZ) of the geometry optimized structures. CCDC 2284285 contains the supplementary crystallographic data for this paper. This data can be obtained free of charge via http://www.ccdc.cam.ac.uk/conts/retrieving.html or from the Cambridge Crystallographic Data Centre, 12 Union Road, Cambridge CB2 1EZ, UK; fax: (+44) 1223-336-033; or e-mail: deposit@ccdc.cam.ac.uk. Supplementary data to this article can be found online at https://doi.org/10.1016/j.poly.2024.117310.

Data availability

The data is available in the Supplementary Information

References

[1] J.F. Berry, F.A. Cotton, S.A. Ibragimov, C.A. Murillo, X. Wang, Searching for precursors to metal−metal bonded dipalladium species: a study of Pd$_2^{4+}$ complexes, Inorg. Chem. 44 (2005) 6129–6137, https://doi.org/10.1021/ic050876c.

[2] F.A. Cotton, N.F. Curtis, C.B. Harris, B.F.G. Johnson, S.J. Lippard, J.T. Mague, W. R. Robinson, J.S. Wood, Mononuclear and polynuclear chemistry of rhenium (III): its pronounced homophilicity, Science 145 (1964) 1305–1307, https://doi.org/10.1126/science.145.3638.1305.

[3] F.A. Cotton, Metal-metal bonding in [Re$_2$X$_8$]$^{2-}$ ions and other metal atom clusters, Inorg. Chem. 4 (1965) 334–336, https://doi.org/10.1021/ic50025a016.

[4] F.A. Cotton, M. Matusz, R. Poli, Synthesis, molecular structure and physicochemical properties of M$_2$(form)$_4$ (M = nickel, palladium; form = N,N'-Di-p-tolylformamidinato), Inorg. Chem. 26 (1987) 1472–1474, https://doi.org/10.1021/ic00257a003.

[5] F.A. Cotton, L.M. Daniels, C.A. Murillo, A systematic approach in the preparation of compounds with .sigma.2.pi.4 vanadium-to-vanadium triple bonds: synthesis, reactivity, and structural characterization, Inorg. Chem. 32 (1993) 2881–2885, https://doi.org/10.1021/ic00065a014.

[6] D.M. Roundhill, H.B. Gray, C.M. Che, Pyrophosphito-bridged diplatinum chemistry, Acc. Chem. Res. 22 (1989) 55–61, https://doi.org/10.1021/ar00158a002.

[7] C.M. Che, W.P. Schaefer, H.B. Gray, M.K. Dickson, P.B. Stein, D.M. Roundhill, Novel binuclear platinum(III) octaphosphite complexes, J. Am. Chem. Soc. 104 (1982) 4253–4255, https://doi.org/10.1021/ja00379a038.

[8] T.A. Stephenson, G. Wilkinson, New ruthenium carboxylate complexes, J. Inorg. Nucl. Chem. 28 (1966) 2285–2291, https://doi.org/10.1016/0022-1902(66)80118-5.

[9] J.L. Bear, Y. Li, B. Han, K.M. Kadish, Synthesis, molecular structure, and electrochemistry of a paramagnetic diruthenium(III) complex. Characterization of Ru$_2$(Hpp)$_4$Cl$_2$, where Hpp is the 1,3,4,6,7,8- hexahydro-2H-pyrimido[1,2-a] pyrimidinate Ion, Inorg. Chem. 35 (1996) 1395–1398, https://doi.org/10.1021/ic950956o.

[10] F.A. Cotton, J. Gu, C.A. Murillo, D.J. Timmons, The first dinuclear complex of palladium(III), J. Am. Chem. Soc. 120 (1998) 13280–13281, https://doi.org/10.1021/ja9832313.

[11] F.A. Cotton, L.M. Daniels, C.A. Murillo, D.J. Timmons, C.C. Wilkinson, The extraordinary ability of guanidinate derivatives to stabilize higher oxidation numbers in dimetal units by modification of redox potentials: structures of Mo$_2^{5+}$ and Mo$_2^{6+}$ compounds, J. Am. Chem. Soc. 124 (2002) 9249–9256, https://doi.org/10.1021/ja0266464.

[12] N.S. Lewis, K.R. Mann, J.G. Gordon, H.B. Gray, Oligomerization and two-center oxidative addition reactions of a dimeric rhodium(I) complex, J. Am. Chem. Soc. 98 (1976) 7461–7463, https://doi.org/10.1021/ja00439a078.

[13] J.P. Fackler, Metal-metal bond formation in the oxidative addition to dinuclear gold(I) species. Implications from dinuclear and trinuclear gold chemistry for the oxidative addition process generally, Polyhedron 16 (1997) 1–17, https://doi.org/10.1016/0277-5387(96)00190-8.

[14] P. Müller, C. Fruit, Enantioselective catalytic aziridinations and asymmetric nitrene insertions into CH bonds, Chem. Rev. 103 (2003) 2905–2920, https://doi.org/10.1021/cr020043t.

[15] H.M.L. Davies, J.R. Manning, Catalytic C–H functionalization by metal carbenoid and nitrenoid insertion, Nature 451 (2008) 417–424, https://doi.org/10.1038/nature06485.

[16] T. Miyazawa, T. Suzuki, Y. Kumagai, K. Takizawa, T. Kikuchi, S. Kato, A. Onoda, T. Hayashi, Y. Kamei, F. Kamiyama, M. Anada, M. Kojima, T. Yoshino, S. Matsunaga, Chiral paddle-wheel diruthenium complexes for asymmetric catalysis, Nat. Catal. 3 (2020) 851–858, https://doi.org/10.1038/s41929-020-00513-w.

[17] D.C. Powers, T. Ritter, Bimetallic Pd(III) complexes in palladium-catalysed carbon–heteroatom bond formation, Nat. Chem. 1 (2009) 302–309, https://doi.org/10.1038/nchem.246.

[18] D.C. Powers, D. Benitez, E. Tkatchouk, W.A. Goddard, T. Ritter, Bimetallic reductive elimination from dinuclear Pd(III) complexes, J. Am. Chem. Soc. 132 (2010) 14092–14103, https://doi.org/10.1021/ja1036644.

[19] Y.B. Dudkina, K.V. Kholin, T.V. Gryaznova, D.R. Islamov, O.N. Kataeva, I. K. Rizvanov, A.I. Levitskaya, O.D. Fominykh, M.Y. Balakina, O.G. Sinyashin, Y. H. Budnikova, Redox trends in cyclometalated palladium(II) complexes, Dalt. Trans. 46 (2017) 165–177, https://doi.org/10.1039/C6DT03786K.

[20] M. Munakata, M. Maekawa, S. Kitagawa, M. Adachi, H. Masuda, Synthesis, properties and crystal structures of dicopper(I) and disilver(I) complexes with 1,8-naphthyridine (napy): [Cu$_2$(napy)$_2$](ClO$_4$)$_2$ and [Ag$_2$(napy)$_2$](ClO$_4$)$_2$, Inorg. Chim. Acta 167 (1990) 181–188, https://doi.org/10.1016/S0020-1693(00)80495-8.

[21] W.P. Griffith, T.Y. Koh, A.J.P. White, D.J. Williams, Two new complexes of 1,8-naphthyridine (napy): The X-ray crystal structures of [OsO$_4$(napy)] (1) and of [Ag$_2$(μ-napy)$_2$(NO$_3$)$_2$] (2), Polyhedron 14 (1995) 2019–2025, https://doi.org/10.1016/0277-5387(95)00041-P.

[22] M. Maekawa, M. Munakata, S. Kitagawa, T. Kuroda-Sowa, Y. Suenaga, M. Yamamoto, Synthesis and crystal structure of two ternary dicopper(I) complexes having the unsymmetrical coordination arrangement bridged by 1,8-naphthyridine (napy). [Cu$_2$(napy)$_2$(Me$_2$CO)](PF$_6$)$_2$·2Me$_2$CO and [Cu$_2$(napy)$_2$(dppm)](CH$_3$CN)] (PF$_6$)$_2$, Inorg. Chim. Acta 271 (1998) 129–136. https://doi.org/10.1016/S0020-1693(97)05950-1.

[23] T. Koizumi, K. Tanaka, Synthesis and crystal structures of mono- and dinuclear silver(I) complexes bearing 1,8-naphthyridine ligand, Inorg. Chim. Acta 357 (2004) 3666–3672, https://doi.org/10.1016/j.ica.2004.05.021.

[24] M. Basato, A. Biffis, G. Martinati, C. Tubaro, C. Graiff, A. Tiripicchio, L.A. Aronica, A.M. Caporusso, Cationic complexes of dirhodium(II) with 1,8-naphthyridine: Catalysis of reactions involving silanes, J. Organomet. Chem. 691 (2006) 3464–3471, https://doi.org/10.1016/j.jorganchem.2006.04.030.

[25] C. Tubaro, G. Greggio, S. Antonello, C. Graiff, A. Biffis, Homoleptic mono- and dinuclear complexes of platinum(II) with 1,8-naphthyridine, Inorg. Chim. Acta 466 (2017) 578–583, https://doi.org/10.1016/j.ica.2017.07.023.

[26] D. Gatteschi, C. Mealli, L. Sacconi, Binuclear complex of 1.5 valent nickel, J. Am. Chem. Soc. 95 (1973) 2736–2738, https://doi.org/10.1021/ja00789a083.

[27] C. Mealli, F. Zanobini, X-Ray crystal structure of the antiferromagnetic binuclear dichloro-μ-dichloro-μ-di(1,8-naphthyridine)-dicopper complex, J. Chem. Soc. Chem. Commun. (1982) 97–98, https://doi.org/10.1039/C39820000097.

[28] A. Tiripicchio, M.T. Camellini, R. Usón, L.A. Oro, M.A. Ciriano, F. Viguri, Complexes of rhodium(I) with 1,8-naphthyridine and related ligands. Crystal structure of [Rh$_2$(μ-napy)$_2$(nbd)$_2$][ClO$_4$]$_2$·H$_2$O, J. Chem. Soc., Dalt. Trans. (1984) 125–131, https://doi.org/10.1039/DT9840000125.

[29] A.E.M. Boelrijk, M.M. van Velzen, T.X. Neenan, J. Reedijk, H. Kooijman, A.L. Spek, A novel dinuclear ruthenium-1,8-naphthyridine catalyst for the oxidation of alcohols and the epoxidation of alkenes, J. Chem. Soc. Chem. Commun. (1995) 2465, https://doi.org/10.1039/c39950002465.

[30] A. Døssing, S. Larsen, A. Van Lelieveld, R.M. Bruun, Preparation and crystal structure of tetrakis-(μ-1,8-naphthyridine)dimolybdenum(II) tetrafluoroborate, Acta Chem. Scand. 53 (1999) 230–234, https://doi.org/10.3891/ACTA.CHEM.SCAND.53-0230.

[31] A. Bencini, E. Berti, A. Caneschi, D. Gatteschi, E. Giannasi, I. Invernizzi, Electronic structure and nature of the ground state of the mixed-valence binuclear tetra(μ-1,8-naphthyridine-N,N')-bis(halogenonickel) tetraphenylborate complexes: experimental and DFT characterization, Chem. - A Eur. J. 8 (2002) 3660, https://doi.org/10.1002/1521-3765(20020816)8:16<3660::AID-CHEM3660>3.0.CO;2-H.

[32] J.D. Aguirre, D.A. Lutterman, A.M. Angeles-Boza, K.R. Dunbar, C. Turro, Effect of axial coordination on the electronic structure and biological activity of dirhodium (II,II) complexes, Inorg. Chem. 46 (2007) 7494–7502, https://doi.org/10.1021/ic700708g.

[33] J.M. Casas, B.E. Diosdado, J. Forniés, A. Martín, A.J. Rueda, A.G. Orpen, Synthesis of binuclear platinum complexes containing the ligands 8-naphthyridine, 2-aminopyridine, and 7-azaindolate. an experimental study of the steric hindrance of the bulky pentafluorophenyl ligands in the synthesis of binuclear complexes, Inorg. Chem. 47 (2008) 8767–8775, https://doi.org/10.1021/ic8006475.

[34] P. Singh, A. Clearfield, I. Bernal, The crystal and molecular structure of an octacoordinated iron(II) compound—tetrakis(1,8-naphthyridine)Fe(II) perchlorate, J. Coord. Chem. 1 (1971) 29–37, https://doi.org/10.1080/00958977108070741.

[35] R.L. Bodner, D.G. Hendricker, Complexes of 1,8-naphthyridines. VII. Eight coordinate transition metal perchlorate complexes of 1,8-naphthyridine, Inorg. Chem. 12 (1973) 33–37, https://doi.org/10.1021/ic50119a009.

[36] T.J. Steiman, C. Uyeda, Reversible substrate activation and catalysis at an intact metal–metal bond using a redox-active supporting ligand, J. Am. Chem. Soc. 137 (2015) 6104–6110, https://doi.org/10.1021/jacs.5b03092.

[37] D.-H. Kwon, M. Proctor, S. Mendoza, C. Uyeda, D.H. Ess, Catalytic dinuclear nickel spin crossover mechanism and selectivity for alkyne cyclotrimerization, ACS Catal. 7 (2017) 4796–4804, https://doi.org/10.1021/acscatal.7b00978.

[38] A.K. Maity, A.E. Kalb, M. Zeller, C. Uyeda, A dinickel catalyzed cyclopropanation without the formation of a metal carbene intermediate, Angew. Chemie Int. Ed. 60 (2021) 1897–1902, https://doi.org/10.1002/anie.202011602.

[39] Y.-Y. Zhou, D.R. Hartline, T.J. Steiman, P.E. Fanwick, C. Uyeda, Dinuclear nickel complexes in five states of oxidation using a redox-active ligand, Inorg. Chem. 53 (2014) 11770–11777, https://doi.org/10.1021/ic5020785.

[40] E. Kounalis, M. Lutz, D.L.J. Broere, Tuning the bonding of a μ-mesityl ligand on dicopper(I) through a proton-responsive expanded PNNP pincer ligand, Organometallics 39 (2020) 585–592, https://doi.org/10.1021/acs.organomet.9b00829.

[41] P.H. van Langevelde, E. Kounalis, L. Killian, E.C. Monkcom, D.L.J. Broere, D.G. H. Hetterscheid, Mechanistic investigations into the selective reduction of oxygen

by a multicopper oxidase T3 site-inspired dicopper complex, ACS Catal. 13 (2023) 5712–5722, https://doi.org/10.1021/acscatal.3c01143.

[42] C.B. van Beek, N.P. van Leest, M. Lutz, S.D. de Vos, R.J.M. Klein Gebbink, B. de Bruin, D.L.J. Broere, Combining metal–metal cooperativity, metal–ligand cooperativity and chemical non-innocence in diiron carbonyl complexes, Chem. Sci. 13 (2022) 2094–2104. https://doi.org/10.1039/D1SC05473B.

[43] M. Smith, Z. Li, L. Landry, K.M. Merz, P. Li, Consequences of overfitting the van der Waals radii of ions, J. Chem. Theory Comput. 19 (2023) 2064–2074, https://doi.org/10.1021/acs.jctc.2c01255.

[44] F.A. Cotton, M. Matusz, R. Poli, X. Feng, Dinuclear formamidinato complexes of nickel and palladium, J. Am. Chem. Soc. 110 (1988) 1144–1154, https://doi.org/10.1021/ja00212a024.

[45] J.F. Berry, E. Bill, E. Bothe, F.A. Cotton, N.S. Dalal, S.A. Ibragimov, N. Kaur, C. Y. Liu, C.A. Murillo, S. Nellutla, J.M. North, D. Villagrán, A fractional bond order of $1/2$ in Pd_2^{5+} −formamidinate species; The value of very high-field EPR spectra, J. Am. Chem. Soc. 129 (2007) 1393–1401, https://doi.org/10.1021/ja067328y.

[46] D.T.U.C. Center, DTU Computing Center resources, 2022. https://doi.org/10.48714/DTU.HPC.0001.

[47] F. Neese, Software update: The ORCA program system—Version 5.0, WIREs Comput. Mol. Sci. 12 (2022) e1606.

[48] J.E. Bercaw, A.C. Durrell, H.B. Gray, J.C. Green, N. Hazari, J.A. Labinger, J. R. Winkler, Electronic structures of Pd^{II} dimers, Inorg. Chem. 49 (2010) 1801–1810, https://doi.org/10.1021/ic902189g.

[49] J.T. Carrano, S.C. Wait, Vibrational spectrum and assignments for 1,6- and 1,8-naphthyridine, J. Mol. Spectrosc. 46 (1973) 401–418, https://doi.org/10.1016/0022-2852(73)90053-2.

[50] W.P. Griffith, T.Y. Koh, SERS of 1,8-naphthyridine and the Raman spectra of two of its complexes, J. Raman Spectrosc. 26 (1995) 1067–1070, https://doi.org/10.1002/jrs.1250261208.

[51] J.R. Durig, B.R. Mitchell, D.W. Sink, J.N. Willis, A.S. Wilson, Far infrared spectra of palladium compounds—II Pyridine and 2,2′-bipyridyl complexes of palladium (II) and platinum (II), Spectrochim. Acta Part A Mol. Spectrosc. 23 (1967) 1121–1135, https://doi.org/10.1016/0584-8539(67)80035-7.

[52] B. Morzyk-Ociepa, K. Dysz, I. Turowska-Tyrk, D. Michalska, New trans-dichloropalladium(II) complexes of 7-azaindole: Crystal and molecular structures, FT-IR, FT-Raman and DFT studies, J. Mol. Struct. 1103 (2016) 202–211, https://doi.org/10.1016/j.molstruc.2015.09.019.

[53] G.R. Fulmer, A.J.M. Miller, N.H. Sherden, H.E. Gottlieb, A. Nudelman, B.M. Stoltz, J.E. Bercaw, K.I. Goldberg, NMR chemical shifts of trace impurities: common laboratory solvents, organics, and gases in deuterated solvents relevant to the organometallic chemist, Organometallics 29 (2010) 2176–2179, https://doi.org/10.1021/om100106e.

[54] S. Prawer, R.J. Nemanich, Raman spectroscopy of diamond and doped diamond, Philos. Trans. R. Soc. London. Ser. A Math. Phys. Eng. Sci. 362 (2004) 2537–2565. https://doi.org/10.1098/rsta.2004.1451.

[55] R.W. Berg, T. Nørbygaard, Wavenumber calibration of CCD detector raman spectrometers controlled by a sinus arm drive, Appl. Spectrosc. Rev. 41 (2006) 165–183, https://doi.org/10.1080/05704920500510786.

[56] C. Liu, R.W. Berg, Determining the spectral resolution of a charge-coupled device (CCD) Raman instrument, Appl. Spectrosc. 66 (2012) 1034–1043, https://doi.org/10.1366/11-06508.

[57] O.V. Dolomanov, L.J. Bourhis, R.J. Gildea, J.A.K. Howard, H. Puschmann, *OLEX2*: a complete structure solution, refinement and analysis program, J. Appl. Cryst. 42 (2009) 339–341, https://doi.org/10.1107/S0021889808042726.

[58] L.J. Bourhis, O.V. Dolomanov, R.J. Gildea, J.A.K. Howard, H. Puschmann, The anatomy of a comprehensive constrained, restrained refinement program for the modern computing environment – *Olex2* dissected, Acta Crystallogr. Sect. A Found. Adv. 71 (2015) 59–75, https://doi.org/10.1107/S2053273314022207.

[59] G.M. Sheldrick, *SHELXT* – Integrated space-group and crystal-structure determination, Acta Crystallogr. Sect. A Found. Adv. 71 (2015) 3–8, https://doi.org/10.1107/S2053273314026370.

[60] F. Neese, F. Wennmohs, U. Becker, C. Riplinger, The ORCA quantum chemistry program package, J. Chem. Phys. 152 (2020) 224108, https://doi.org/10.1063/5.0004608.

[61] J.P. Perdew, S. Kurth, A. Zupan, P. Blaha, Accurate density functional with correct formal properties: a step beyond the generalized gradient approximation, Phys. Rev. Lett. 82 (1999) 2544–2547, https://doi.org/10.1103/PhysRevLett.82.2544.

[62] A. Schäfer, H. Horn, R. Ahlrichs, Fully optimized contracted Gaussian basis sets for atoms Li to Kr, J. Chem. Phys. 97 (1992) 2571–2577, https://doi.org/10.1063/1.463096.

[63] F. Weigend, M. Häser, H. Patzelt, R. Ahlrichs, RI-MP2: optimized auxiliary basis sets and demonstration of efficiency, Chem. Phys. Lett. 294 (1998) 143–152, https://doi.org/10.1016/S0009-2614(98)00862-8.

[64] D. Andrae, U. Häußermann, M. Dolg, H. Stoll, H. Preuß, Energy-adjustedab initio pseudopotentials for the second and third row transition elements, Theor. Chim. Acta 77 (1990) 123–141, https://doi.org/10.1007/BF01114537.

[65] M.E. Casida, Time-dependent density functional response theory for molecules, in: Recent Adv. Density Funct. Methods, World Scientific, 1995, pp. 155–192. https://doi.org/10.1142/9789812830586_0005.

[66] D. Rappoport, F. Furche, Property-optimized Gaussian basis sets for molecular response calculations, J. Chem. Phys. 133 (2010) 134105, https://doi.org/10.1063/1.3484283.

[67] B. Helmich-Paris, B. de Souza, F. Neese, R. Izsák, An improved chain of spheres for exchange algorithm, J. Chem. Phys. 155 (2021) 104109, https://doi.org/10.1063/5.0058766.